JACS
JOURNAL OF THE AMERICAN CHEMICAL SOCIETY
Article
pubs.acs.org/JACS

Sequence-Dependent Structure/Function Relationships of Catalytic Peptide-Enabled Gold Nanoparticles Generated under Ambient Synthetic Conditions

Nicholas M. Bedford,[*,†,‡,§,×] Zak E. Hughes,[⊥,×] Zhenghua Tang,[§,∥] Yue Li,[#] Beverly D. Briggs,[§,•] Yang Ren,[▽] Mark T. Swihart,[#] Valeri G. Petkov,[⊗] Rajesh R. Naik,[*,‡] Marc R. Knecht,[*,§] and Tiffany R. Walsh[*,⊥]

[†]Applied Chemical and Materials Division, National Institute of Standards and Technology, Boulder, Colorado 80305, United States
[‡]Materials and Manufacturing Directorate, Air Force Research Laboratory, Wright-Patterson AFB, Ohio 45433, United States
[§]Department of Chemistry, University of Miami, Coral Gables, Florida 33146, United States
[⊥]Institute for Frontier Materials, Deakin University, Geelong, Victoria 3216, Australia
[∥]New Energy Research Institute, School of Environment and Energy, South China University of Technology, Guangzhou Higher Education Mega Centre, Guangzhou 510006, China
[#]Chemical and Biological Engineering, State University of New York at Buffalo, Buffalo, New York 14260, United States
[▽]Advanced Photon Source, Argonne National Laboratory, Argonne, Illinois 60439, United States
[⊗]Department of Physics, Central Michigan University, Mt. Pleasant, Michigan 48858, United States

Supporting Information

ABSTRACT: Peptide-enabled nanoparticle (NP) synthesis routes can create and/or assemble functional nanomaterials under environmentally friendly conditions, with properties dictated by complex interactions at the biotic/abiotic interface. Manipulation of this interface through sequence modification can provide the capability for material properties to be tailored to create enhanced materials for energy, catalysis, and sensing applications. Fully realizing the potential of these materials requires a comprehensive understanding of sequence-dependent structure/function relationships that is presently lacking. In this work, the atomic-scale structures of a series of peptide-capped Au NPs are determined using a combination of atomic pair distribution function analysis of high-energy X-ray diffraction data and advanced molecular dynamics (MD) simulations. The Au NPs produced with different peptide sequences exhibit varying degrees of catalytic activity for the exemplar reaction 4-nitrophenol reduction. The experimentally derived atomic-scale NP configurations reveal sequence-dependent differences in structural order at the NP surface. Replica exchange with solute-tempering MD simulations are then used to predict the morphology of the peptide overlayer on these Au NPs and identify factors determining the structure/catalytic properties relationship. We show that the amount of exposed Au surface, the underlying surface structural disorder, and the interaction strength of the peptide with the Au surface all influence catalytic performance. A simplified computational prediction of catalytic performance is developed that can potentially serve as a screening tool for future studies. Our approach provides a platform for broadening the analysis of catalytic peptide-enabled metallic NP systems, potentially allowing for the development of rational design rules for property enhancement.

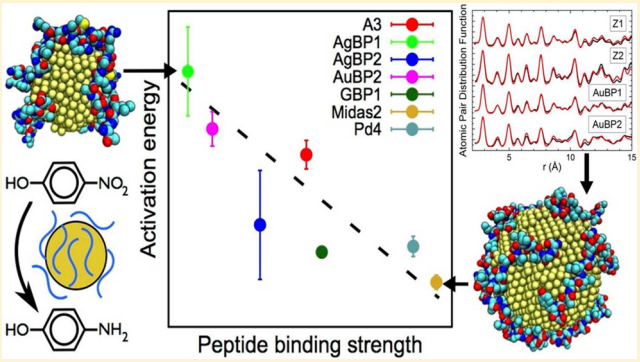

INTRODUCTION

Bio-enabled routes for nanomaterial synthesis and assembly comprise an area of increasing interest as a versatile strategy to create materials with enhanced and emergent properties under environmentally benign conditions.[1−4] The complexity, specificity, and materials recognition properties of biomolecules allow for potential rational design routes that are not readily achieved using conventional nanoparticle (NP)/ligand combinations. For example, the complementary nature of DNA base pairs and the helical structure of the duplex have provided a means to rationally create sophisticated assemblies of nanomaterials.[5−7] In addition, proteins and peptides have demonstrated the capability to direct the nucleation, growth, and organization of inorganic nanomaterials in aqueous solution at room temperature, while imparting sequence- and structure-dependent shape,

Received: September 9, 2015
Published: December 17, 2015

DOI: 10.1021/jacs.5b09529
J. Am. Chem. Soc. 2016, 138, 540−548

size, and/or materials property control through biomolecular self-assembly and specific motif recognition.[4,8−15] Peptides are particularly advantageous for NP synthesis, in that minor alternations to a peptide sequence can yield materials with drastically different shapes, sizes, and properties,[2,14,16−18] allowing for the development of sequence-driven design rules.

While the prospects for green, peptide-enabled approaches to the manipulation of NP properties are exciting, an in-depth understanding of sequence-dependent structure/function relationships is vital to establishing rational bio-inspired design rules. As such, the nature of the biotic/abiotic interface of various inorganic surfaces has been the focus of intense experimental and computational investigations to determine how the overall ensemble of peptide structures at this interface can influence the properties of the nanomaterial.[19−25] While these efforts have provided valuable fundamental insights into peptide−nanomaterial interactions, the underlying assumption in most cases has been that the inorganic component is a perfectly ordered truncate of the parent crystalline material. For peptide-directed NP synthesis, the presence of different binding motifs in the peptide could potentially influence the atomic scale structure at the particle surface, thus causing structural differences that can impart sequence-dependent material properties. In the case of peptide-capped Pd NPs, a recent study demonstrated that single or double mutations of a bio-combinatorially derived Pd-binding peptide (termed Pd4)[26] produced varying degrees of surface structural disorder of the Pd NP as determined by synchrotron radiation methods.[2] Using these experimentally derived structures, molecular dynamics (MD) simulations were used to relax the NP surface atoms and model the interaction of the peptides at the non-ideal Pd particle surfaces. Using this tandem approach, a direct correlation between the catalytic properties and sequence-dependent surface disorder was elucidated. This approach provides an avenue for potentially establishing peptide sequence-based rational design rules for producing nanomaterials with tunable properties; however, full realization of this promise will require substantial and systematic sequence manipulation and comprehensive exploration of other material systems.

In this contribution, we elucidate sequence-dependent structure/function relationships through integrated experimental characterization and advanced molecular simulations, applied to a series of peptide-promoted catalytic Au NPs (PEPCANs) that exhibit varying catalytic activities for 4-nitrophenol reduction under aqueous conditions, room temperature, and ambient pressure.[13] Using previously isolated noble metal binding peptides,[26−32] Au NPs were synthesized in aqueous solution, using only the binding peptide to cap particle growth and $NaBH_4$ as a reducing agent. The peptide sequences associated with this set of PEPCANs contain a variety of residue functionalities and sequence lengths, providing an opportunity to explore diverse sequence-driven structural changes. Using atomic pair distribution function (PDF) analysis of high-energy X-ray diffraction (HE-XRD) patterns, the atomic-scale structure of the NPs associated with each PEPCAN was probed, revealing significant structural variations. Reverse Monte Carlo (RMC) simulations guided by the experimental PDF data yielded NP structural models with varying degrees of surface disorder: a stark contrast from commonly assumed NP truncates of the bulk crystal structure. Using these configurations, state-of-the-art, multi-chain replica-exchange with solute tempering (REST)[33,34] molecular dynamics (MD) simulations were performed to predict the ensemble of likely overlayer structures adsorbed at the NP surface for each PEPCAN, and to provide detailed molecular-level insights into the biotic/abiotic interface. Advanced conformational sampling approaches are pivotal to making reliable predictions, because all of the materials-binding peptides considered in this work are thought to be intrinsically disordered in character (i.e., intrinsically disordered peptides, or IDPs).[13,19] The corresponding potential energy landscape of such IDP-like systems is anticipated to be highly complex;[35] even for the adsorption of a single peptide chain, there is no single "configuration" that can describe this state.[19] The presence of several adsorbed peptide chains in each overlayer will admit many different possible arrangements. Standard MD approaches cannot deliver sufficient conformational sampling of these systems[19] and may give rise to misleading conclusions. The need for extensive conformational sampling is further exacerbated by the need to use an explicit description of water since the use of implicit solvent is highly problematic for IDPs.[36] REST MD simulations of surface-adsorbed peptides have been previously shown to be a computationally tractable approach for exploring the potential energy landscape of materials-adsorbed peptides in aqueous media, and have aided the elucidation the structure/function behaviors of such systems,[19,23,34,37] providing excellent agreement with experimental findings.[38,39]

The resulting NP-adsorbed peptide overlayer configurations predicted from our REST simulations were then used to elucidate links between the structural and dynamic properties and the catalytic activity of the NPs, through which structure/function relationships were established. The activity for 4-nitrophenol reduction, a surface-driven reaction,[40] was found to depend upon several structural and dynamic aspects of the biotic/abiotic interfaces. Full exploration of these relationships from a computational perspective requires comprehensive sampling of the conformational ensemble of the PEPCAN overlayer, to probe both the enthalpic and entropic contributions to the peptide-NP binding. Such a rigorous tandem experimental/computational approach provides unprecedented levels of structural information necessary to clearly evaluate the interactions at the biotic/abiotic interface, providing a platform to potentially achieve rational NP design through peptide-enabled methodologies.

EXPERIMENTAL SECTION

Peptide Synthesis. Peptides were synthesized using an automated TETRAS model synthesizer (Creosalus) following standard solid-phase Fmoc protocols.[41] Crude peptides were purified using reverse-phase HPLC and confirmed using MALDI-TOF mass spectrometry. Upon confirmation, peptide solutions were lyophilized and stored at −80 °C prior to use.

Nanoparticle Synthesis. Au NPs were synthesized as previously described.[13] Briefly, 500 μL of a 1.0 mM solution of peptide was added to 4.46 mL of water. To this solution 10 μL of 0.1 M $HAuCl_4$ was added. This solution was vigorously stirred for 10 min, followed by the addition of 30 μL of freshly prepared 0.1 M $NaBH_4$ in water to reduce the Au^{3+} to Au^0. The reduction reaction was allowed to proceed unperturbed for at least 1 h prior to characterization or catalytic testing. A peptide-to-Au ratio of 1:2 and a $NaBH_4$-to-Au ratio of 3:1 were used for all syntheses. Double-distilled, 18.2 MΩ·cm water was used in all experiments.

HE-XRD and Atomic PDF Analysis. HE-XRD patterns were obtained at the 11-ID-C beamline of the Advanced Photon Source, Argonne National Laboratory, using X-rays with an energy of 115 keV. Lyophilized Au NP samples were loaded into 2.0 mm diameter quartz capillaries, and diffracted X-ray intensities were collected by a large area detector. HE-XRD patterns were corrected for background scattering,

DOI: 10.1021/jacs.5b09529
J. Am. Chem. Soc. 2016, 138, 540−548

Table 1. Summary of Peptides Used for Au NP Synthesis, Binding Characteristics, NP Size, Catalytic Activity, and Atomic-Level Metrics at the Biotic/Abiotic Interface

peptide	sequence	p*I*[a]	Δ*G* (kJ/mol)[b]	particle size (nm)[c]	E_a (kJ/mol)[d]	Ω_{NP}[e]	Ω_{111}[e]	$SASA_{NP}$(nm)[f]	no. atoms CN < 7[g]
A3	AYSSGAPPMPPF	5.57	−31.8 ± 0.3	2.3 ± 0.5	20.0 ± 1.0	−2.51	−2.63	15.6 ± 0.6	72
AgBP1	TGIFKSARAMRN	12.01	−31.6 ± 0.2	3.2 ± 0.7	25.8 ± 3.1	−2.67	−3.55	22.6 ± 1.3	98
AgBP2	EQLGVRKELRGV	8.85	−35.3 ± 1.2	3.6 ± 1.0	15.1 ± 3.8	−3.12	−2.99	30.5 ± 1.5	137
AuBP1	WAGAKRLVLRRE	11.71	−37.6 ± 0.9	4.2 ± 1.1	N/A	−3.21	−3.79	27.3 ± 1.7	141
AuBP2	WALRRSIRRQSY	12	−36.4 ± 0.3	3.8 ± 0.8	21.8 ± 1.2	−3.19	−3.36	32.7 ± 1.2	181
GBP1	MHGKTQATSGTIQS	8.52	−37.6 ± 1.0	3.2 ± 0.8	13.2 ± 0.4	−2.33	−2.51	24.6 ± 1.3	106
Midas2	TGTSVLIATPYV	5.18	−35.7 ± 1.2	5.1 ± 1.6	11.1 ± 0.5	−1.95	−1.62	59.9 ± 1.7	237
Pd4	TSNAVHPTLRHL	9.47	−30.3 ± 0.2	4.3 ± 1.7	13.6 ± 0.7	−2.15	−1.80	38.3 ± 1.5	170
Z1	KHKHWHW	10.00	−31.3 ± 0.1	3.9 ± 0.9	N/A	−2.06	−2.22	44.9 ± 1.5	172
Z2	RMRMKMK	12.02	−35.0 ± 0.6	4.9 ± 1.5	9.1 ± 0.1	−2.78	−2.31	60.8 ± 2.4	262

[a] p*I* values calculated from web.expasy.org/compute_pi/. [b] Free energy of binding on polycrystalline Au substrate determined by quartz crystal microbalance.[19] [c] Determined by image analysis of TEM micrographs.[13] [d] Activation energy of 4-nitrophenol reduction to 4-aminophenol in the presence of $NaBH_4$.[13] [e] Estimated enthalpic component determined from simulation data.[19] See text for details. [f] Solvent-accessible surface area of Au NP, determined from simulation data. [g] The number of Au atoms with Au−Au coordination number of <7, determined from simulation data.

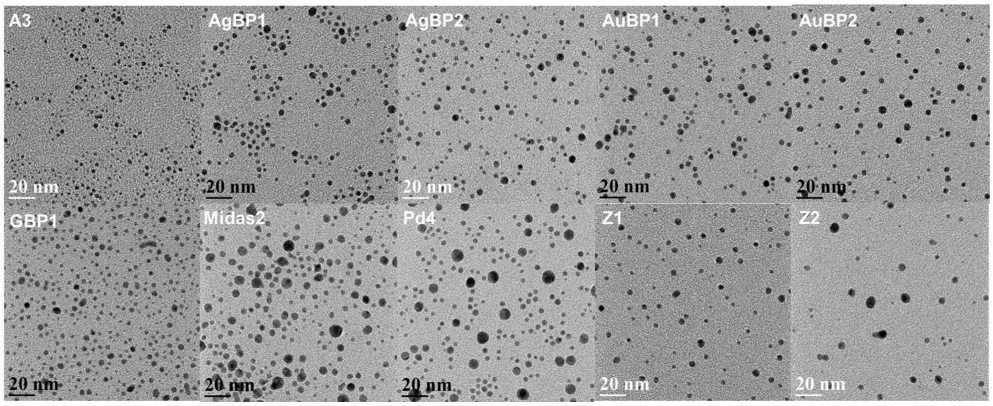

Figure 1. Representative TEM images of each PEPCAN examined in this study.

converted into Q[S(Q)-1], and Fourier transformed into PDFs using the program RAD.[42]

RMC Modeling. RMC simulations were performed with the help of the program RMC++.[43] Initial configurations were created using atomic configurations of the size determined by TEM imaging and the known structure of fcc bulk Au.[44] Simulations were run with various first Au−Au pair distances and coordination number constraints[45] to prevent unrealistic NPs structures. This process is repeated until the computed PDF converges to the experimental PDF data in very good detail, with typical agreement factors (R_w) below ∼10% (see Table S1, Supporting Information).

Replica Exchange with Solute Tempering Molecular Simulations. REST MD simulations were performed for all 10 aqueous PEPCANs outlined in Table 1. Each PEPCAN system comprised the Au NP structure obtained from the RMC simulations, a number of adsorbed peptide chains (see below), liquid water, and a sufficient number of Cl^- counter-ions to neutralize the overall charge of the simulation cell. The number of peptide chains in each system was varied such that the NP surface coverage was kept approximately constant. Full details of each system are given in Table S5. The simulations were performed using GROMACS v5.0.[46] A modified version of the CHARMM-METAL force-field (FF) was used to describe the interatomic interactions (see Supporting Information, Section S4, for full details). The simulations were performed in the isothermal−isobaric (*NpT*) ensemble, using 16−32 replicas (depending on system size) spanning a 300−500 K temperature window. All simulations were run for 20×10^6 REST MD steps. The systems had between 50 965 and 95 346 atoms per replica. Additional information on the simulation details are described in the Supporting Information, Section S2.

Simulation Analysis. The Boltzmann-weighted ensemble of peptide conformations at 300 K was analyzed from the perspective of peptide/NP contact, structural clustering analyses, and the dictionary of secondary structure prediction secondary structural analysis. We also analyzed the structure of the Au NPs, via calculation of the solvent-available surface area (SASA), the number of low-coordinate Au surface atoms, and the number of low-coordinate Au surface atoms exposed to solvent. Full details of all simulation analyses can be found in the Supporting Information, Section S3.

RESULTS AND DISCUSSION

PEPCANs, summarized in Table 1, were synthesized in water using established methods.[13] Transmission electron microscopy (TEM) was used to determine NP size and shape (Figure 1).[13] The NPs were generally spherical in shape and ranged in size from ∼2 to 5 nm, with no clear trend correlating size to peptide length, p*I*, or previously determined free-energy of adsorption onto planar Au surfaces (Table 1).[13] Additionally, trends in size and monodispersity did not correlate with the provenance of the original biopanning target (Au, Ag, or Pd) of the peptide, suggesting peptide specificity does not necessarily influence NP size. These NPs were catalytically active for the reduction of 4-nitrophenol to 4-aminophenol, as demonstrated previously (Table 1).[13] Analysis of peptide chemistry, affinity for Au surfaces, peptide size, and resulting NP size provided no clear trends in either reaction rates or activation energies (see Supporting Information, Figure S1). Therefore, differences in the atomic arrangement at the NP surface, dictated by the capping peptide during Au^{3+} reduction in solution, are likely at the root of the catalytic activity differences. Note that activation

DOI: 10.1021/jacs.5b09529
J. Am. Chem. Soc. 2016, 138, 540−548

energies for AuBP1 and Z1 could not be obtained due to the instability of these PEPCANs at higher temperatures.

HE-XRD coupled to atomic PDF analysis was employed to investigate the detailed structure of PEPCANs. Atomic PDF analysis is ideal for studying the structure of nanomaterials lacking long-range periodic order.[47] PDFs were obtained by converting experimental HE-XRD data (see Figure S2) into total reduced structure functions, $Q[S(Q) - 1]$ (see Figure S3), and Fourier transforming the latter into atomic PDFs, $G(r) = 4\pi r[\rho(r) - \rho_0]$, wherein r is the atomic pair distance and $\rho(r)$ and ρ_0 are the local and average atomic number densities, respectively (see Supporting Information for further details). Peaks in the PDF reflect distances of greater atomic density (compared to the average), while valleys in the PDF correspond to distance of relatively low atomic density. The PDFs for the Au NPs studied here are shown in Figure 2 (black lines).

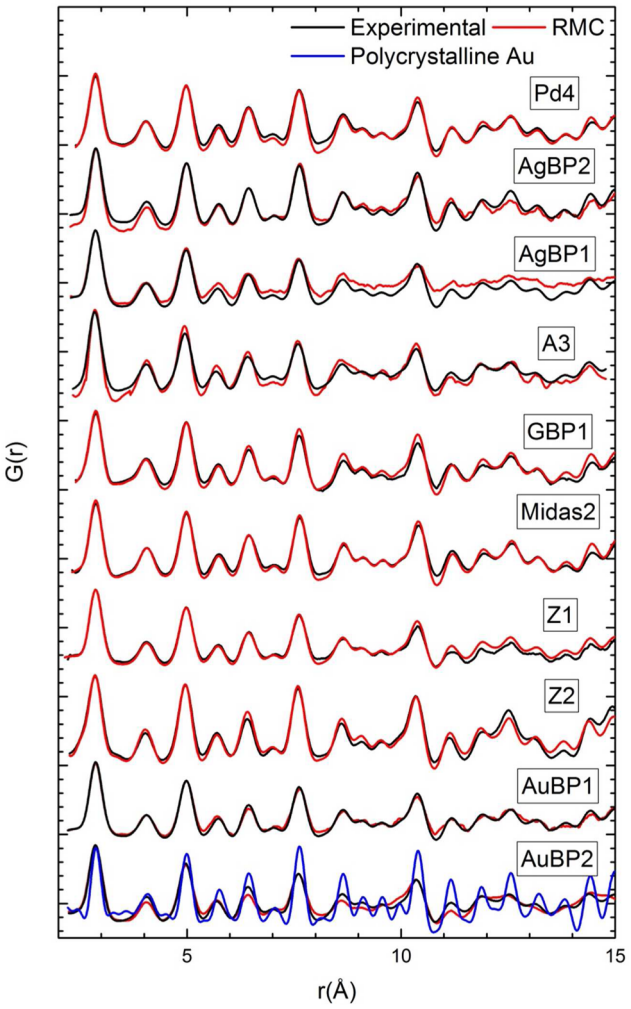

Figure 2. Experimental (black lines) and RMC model-derived (red lines) atomic PDFs for peptide-enabled Au NPs. For reference, an experimental atomic PDF for polycrystalline Au standard is also given (blue line).[48] PDFs are offset by a constant factor for ease of comparison.

Overall, the PDFs exhibit features characteristic of a face-centered cubic (fcc)-type structure with significant sequence-dependent differences in atomic structure at various length scales (see Figure S4), such as decreases in relative intensity, overall peak position, and peak shape. All of these factors collectively reflect the overall structural order in the PEPCANs. The relative decay in peak oscillations over longer interatomic distances signifies an overall decrease in PEPCAN structural order. PDFs for Au NPs made from Z2 exhibit minimal decay compared to those of remaining NPs; PDFs for GBP1, Midas, and Pd4-based NPs extended to somewhat longer r distances, while that for AgBP2-bound NPs exhibited moderately damped oscillations. Finally, the PDFs for the remaining PEPCANs are dampened at longer atomic pair distances, in comparison. Note that this trend does not simply follow a linear trend in peak dampening to PEPCAN size (see Figure S5), indicating that peptide sequence can directly impact the degree of overall structural order in Au PEPCANs. For comparison, an experimental atomic PDF for polycrystalline Au standard (~10 μm particle size, Figure 2, blue line),[48] shows very little dampening at longer atomic pair distances (see Figure S6).

Structure models for PEPCANs were generated by RMC guided by the respective experimental PDFs with the help of the program RMC++ (Figure 2, red lines).[43] In RMC, atoms in model configurations are moved at random and atomic PDFs are recalculated after each move. Moves are accepted or rejected according to the Metropolis criterion,[49] and are repeated until the model-derived PDF converges to the experimental data. RMC is an established approach for building structure models for materials lacking long-range order,[50−52] including NPs.[2,53,54] As evident from Figure 2, the RMC models reasonably reproduced the experimental PDFs, with reported "goodness of fit" parameters, R_w, below 10% (see Table S1 and Section S1 in the Supporting Information). RMC generated structure models are shown in Figure 3. All models exhibit varying

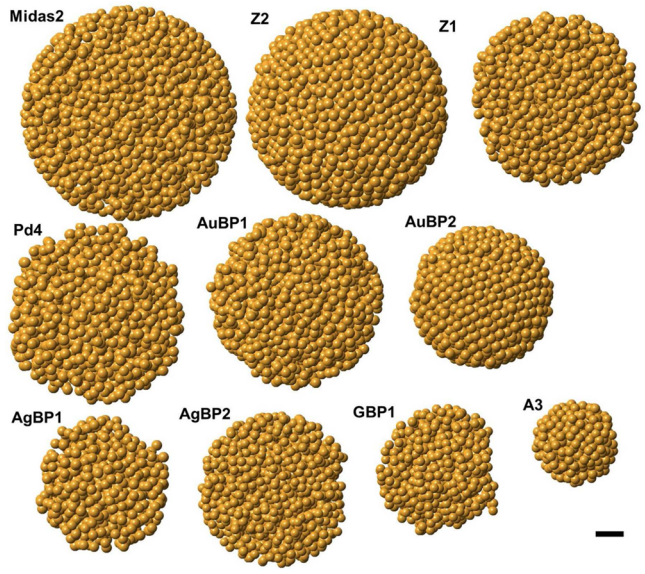

Figure 3. PEPCAN configurations generated by RMC simulations guided by experimental PDF data. Scale bar equals 1 nm.

degrees of surface structural distortions, indicating that differences in the residue content and particular recognition motifs of peptide overlayers impart varying degrees of structural disorder at NP surface. Note that the core atoms within the NPs remain significantly more fcc-like than the surface atoms (Figure S7). The stark difference in structural order between core and surface atoms implies the biotic/abiotic interface heavily influences surface disorder. Qualitatively, AuBP2 and Z2-bound Au PEPCANs appear the most ordered at the surface, while the surface of Au PEPCANs synthesized with AgBP1,

DOI: 10.1021/jacs.5b09529
J. Am. Chem. Soc. 2016, 138, 540−548

AgBP2, GBP1, Pd4, and A3 appears very rough, with a large number of under-coordinated surface atoms clearly visible. These irregular NP surfaces and their related peptide overlayer morphologies directly affect NP catalytic activity (*vide infra*). Note that while single NP configurations are generated from RMC, these configurations are representative of an ensemble of NPs probed during HE-XRD experiments, which yields the experimental PDF. Using NP ensemble-averaged structural features to understand and explain NP ensemble-averaged properties (e.g., catalytic, magnetic, optical, etc.) puts NP atomic structure and catalytic property exploration on the same footing, allowing configurations generated by RMC simulations to be useful in elucidating catalytic properties with additional computational methods.

With ensemble-average atomically resolved PEPCAN structures available from experimental data, advanced simulation techniques can be used to predict the structure of the peptide overlayer adsorbed on the surface of these Au PEPCANs, providing a molecular-level picture of the biotic/abiotic interface. However, the complex potential energy landscape of the adsorbed multi-chain peptide overlayer, involving both peptide−surface interactions and inter-peptide interactions means that particular care must be taken to ensure that the complex conformational space of the peptide chains is sampled sufficiently.[19,23] To accomplish this, we employed the REST approach (see Supporting Information, Methods and Sections S2−S4). Prior to our REST simulations of the biotic/abiotic interface, additional surface relaxation was performed on the RMC-generated structures. Due to the entropic nature of the RMC algorithm and the conflation of the entire ensemble of experimentally determined PEPCAN structures and sizes into a single configuration, a slight overestimation of overall atomic disorder is possible.

After surface relaxation, the solvated Au PEPCANs with the peptide overlayers adsorbed on the PEPCAN surface were modeled in liquid water using REST simulations to generate the ensemble of likely PEPCAN overlayer morphologies. Figure 4a shows exemplar snapshots of the most highly populated configuration of the A3, AgBP1, and GBP1 peptide overlayers adsorbed on Au PEPCANs under aqueous conditions (snapshots of all 10 PEPCAN systems are shown in Figures S8 and S9). One of the few points of experimental comparison for our REST-predicted peptide overlayer structures comprises the circular dichroism (CD) spectroscopy data reported previously.[13] Our secondary structural analysis, averaged over all peptide chains in each PEPCAN, are summarized in Table S16. These results show excellent agreement with these experimental data, indicating that over half of the conformational ensemble in each case is random coil in character.

Possible factors that may influence the catalytic activity of the PEPCANs include the conformational freedom of the individual peptide chains, the conformational freedom of the entire peptide overlayer, the solvent accessible surface area of the Au PEPCAN exposed by the peptide overlayer, the magnitude of the enthalpic contribution of the peptide adsorption to the PEPCAN, and the amount of surface disorder of Au atoms at the metallic surface. The first two factors are principally governed by a balance between the peptide−surface and peptide−peptide interactions. By analyzing structural properties calculated from our predicted ensemble of configurations, we can establish which properties appear to correlate with the catalytic activity of the different PEPCANs. However, given the anticipated complexity associated with these systems, it is perhaps unlikely that a single key property can explain the entire range of catalytic activity of the

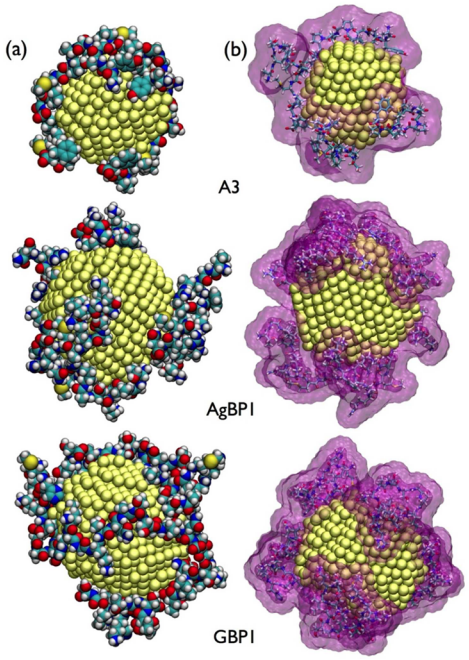

Figure 4. Structural information of exemplar PEPCANs, A3, AgBP1, and GBP1, obtained from the Boltzmann weighted ensemble of configurations predicted by REST-MD simulations, using NP models originally produced by RMC modeling of experimental PDF data. (a) Typical configuration of the most populated cluster of the peptide overlayer. (b) Indication of the exposed NP surface within the peptide overlayer.

PEPCANs. What appears more probable is that the catalytic activity of a PEPCAN is determined from a more complex interplay between several factors. Understanding the sequence-driven relationships between these factors can provide a valuable fundamental basis for development of rational peptide design strategies for optimized catalysts embracing a wider range of catalytic mechanisms. Of the factors listed above, overall, our structural analysis of PEPCANs revealed that several of these exhibited only moderate correlation at best with the observed catalytic activity, as detailed in the Supporting Information, Section S5 (the number of distinct conformations accessed by the individual peptide chains/entire peptide overlayer, referred to herein as the conformational entropy contribution, which showed no correlation) and Section S6 (the solvent-accessible NP surface area, $SASA_{NP}$, and the number of low-coordinate Au sites, $N_{CN\text{-}low}$, both of which showed modest correlation). We also investigated the fraction of low-coordinate surface Au atoms that were in contact with the peptide or solvent, as summarized in Table S15, and found no discernible trend with activation energy. Herein we focus on the factor that showed the strongest correlation with the catalytic activity, namely the enthalpic contribution of the peptide(s) adsorption to the Au NP. We would like to note that possible electronic interactions between amino acid functionalities and surface Au atoms may modulate the reactivity to a certain extent, but a thorough investigation of this topic falls outside the scope of this manuscript and will be the subject of future studies.

Our previous studies[19,23] have also suggested that the presence of non-covalent strongly bound anchor residues can be a key determinant in the adsorption free energy of the surface-bound peptides. It was previously hypothesized that this anchoring effect may exert a strong influence on the formation

DOI: 10.1021/jacs.5b09529
J. Am. Chem. Soc. 2016, 138, 540−548

of the peptide overlayer morphology, thus facilitating the exposure of reactive sites on the Au PEPCAN surface.[13] To explore this hypothesis, we have calculated a relative measure of the influence of the enthalpic contribution to the peptide-surface adsorption, which we have introduced in previous studies.[19,23] Here, we elaborate on this metric by defining a contact score, Ω, for a given peptide as

$$\Omega = \sum_{i=1}^{r} c_i \Delta H_{\mathrm{ads}}^{\mathrm{AA}} \quad (1)$$

where c_i is the fraction of the trajectory that each peptide residue spends in contact with the Au PEPCAN surface (illustrated in Figure 5a for three exemplar peptide sequences),

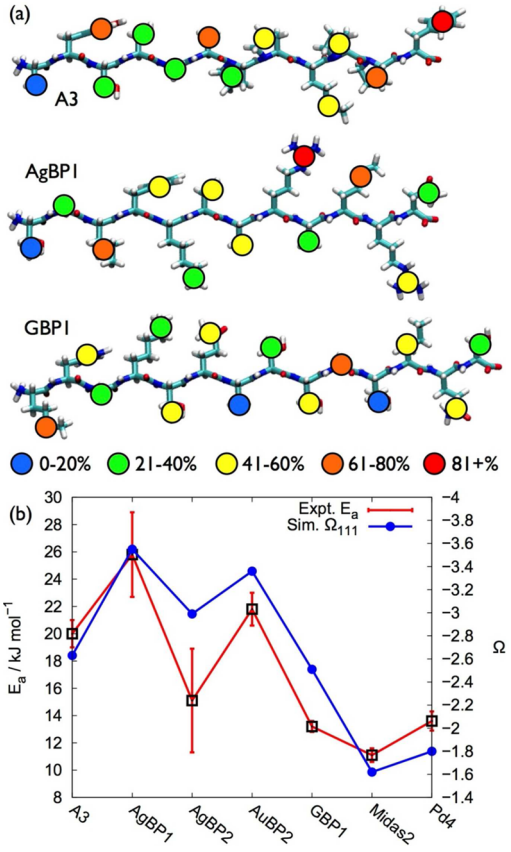

Figure 5. (a) Average degree of residue / Au NP surface contact, indicated by the colored circles, for the A3, AgBP1, and GBP1 peptides. (b) The relationship between the activation energies and the contact score on the aqueous Au(111) interface for peptides at least 12 residues in length.

r is the total number of residues in the peptide sequence, and ΔH_{ads} is the enthalpy of adsorption of the corresponding amino acid.[55] The contact score for each PEPCAN, Ω_{NP}, is then calculated from the average contact scores of all peptide chains present in the PEPCAN. See Supporting Information, Section S7, for more details. The values of Ω_{NP}, as well as the theoretical maximum contact score for a single chain for a given peptide sequence, Ω_{max}, are given in the Table S4. Unlike our conformational entropy analysis, our predictions of Ω_{NP} exhibit some correlation with E_a, as shown in Figure S10a. However, two different classes of behavior were evident: Set A, comprising AgBP1, A3, GBP1, Pd4, and Midas2; and Set B comprising AuBP2, AgBP2, and Z2.

To probe this further, using data taken from previous work[19] we compared the overlayer-averaged contact scores of our PEPCAN overlayers, Ω_{NP}, with the contact scores calculated from REST simulations of a single peptide chain adsorbed at the aqueous planar Au(111) interface, denoted Ω_{111} (see Supporting Information, Section S7 and Table S4). In general, there is very good agreement between Ω_{NP} and Ω_{111}, using our two definitions of the contact scores (see Figure S10c). However, two exceptions to this trend are evident: AgBP1 and AuBP1. Going further, we find excellent agreement between Ω_{111} and E_a for peptides with sequence length of 12 or greater; see Figures 5b and S10b. Shorter peptides, namely Z1 and Z2, supported Au PEPCAN sizes toward the larger end of the scale (Figure 3), and we propose that the relative length-scale of the peptide length to Au PEPCAN size in these instances led to a deviation from the trends seen for the longer peptides (see Figure S10c).

The somewhat superior performance of Ω_{111} can be rationalized by considering the fact that the FF used in our simulations has been specifically parametrized for Au facets, namely the Au(111) and Au(100) surfaces. Figure S11 illustrates the different degrees of faceting found in the underlying Au NPs of the PEPCANs. The Au NPs of the AgBP1 and AuBP1 PEPCANS are among the more disordered and least faceted of the set (see Figure S11a,c), explaining why they show the greatest discrepancy between Ω_{111} and Ω_{NP}. In contrast, AuBP2 has one of the highest degrees of faceting (see Figure S11d). In a similar vein, while GBP1 is more disordered than AuBP2, its corresponding Au NP structure features some reasonably large facets (see Figure S11b), relative to the small size of the Au PEPCAN in this case. Consistent with our proposal, both AuBP2 and GBP1 show good agreement between Ω_{111} and Ω_{NP}. Therefore, it is consistent that our FF performs more reliably for more strongly faceted materials, and suggests that further refinement of the FF to account for highly disordered surfaces may be valuable in future studies. Note that the degree of Au PEPCAN surface disorder observed from the REST simulations of the PEPCANs may differ from those generated by our RMC procedure, for reasons outlined earlier.

Given the complexity of these PEPCAN systems, some interplay between the three chief factors (Ω, $\mathrm{SASA_{NP}}$, and $N_{\mathrm{CN\text{-}low}}$) identified by this study is anticipated. For example, we compared three PEPCANs: derived from A3, AgBP1, and GBP1. For AgBP1 and GBP1, the Au NPs are of an almost equal size (919 and 917 Au atoms, respectively), feature an approximately equal number of low-coordinate Au atoms, and possess similar solvent-accessible surface areas. However, despite these similarities, the GBP1 PEPCAN has a low E_a, while the AgBP1 PEPCAN featured the highest E_a in our set. In this instance, the contact score, Ω, is seen to be decisive, with the magnitude of this score for the AgBP1 case being much greater than that for GBP1 (Ω_{111} = −3.55 and −2.51, for AgBP1 and GBP1, respectively). Another example is the A3 PEPCAN, capped with a known Au- and Ag-binding peptide,[27,56] which featured the smallest Au NP in our set (453 Au atoms) and the lowest overall $\mathrm{SASA_{NP}}$ and $N_{\mathrm{CN\text{-}low}}$ while yielding a mid-range E_a value. Again, the contact score provides resolution, since Ω_{111} = −2.63 for A3, which is significantly lower in magnitude than that of AgBP1, and consistent with our proposed metrics, the A3 PEPCAN is more catalytically active than the AgBP1 system. This indicates that the adsorption behavior of the peptides on the Au NP surface plays a crucial role in determining the catalytic activity of the PEPCAN.

DOI: 10.1021/jacs.5b09529
J. Am. Chem. Soc. 2016, 138, 540−548

Our REST simulations of the PEPCANs in aqueous solution are of an unprecedented size and complexity for this advanced sampling approach, and accordingly, demand substantial supercomputing resources for their successful and timely realization. For example, a 20 ns REST MD simulation for a typical PEPCAN required ∼72 000 CPU-hours and took ∼17 days to run at our supercomputing facility. The REST approach as applied to the PEPCANs is therefore computationally very costly and not practicable for intensive computational screening applications. However, as we have already demonstrated, the contact score, Ω, can be approximated solely on the basis of single-chain properties of the peptide, potentially opening a route for the feasible screening of PEPCANs to identify candidates for a range of surface-mediated catalytic reactions. Because the REST simulation of a single peptide chain adsorbed at the planar Au interface is significantly less computationally demanding than a REST simulation of the PEPCAN (requiring ∼one-fifth of the CPU-hours compared with the PEPCAN), in the future, we can exploit simulations of these relatively simpler planar systems as part of a pre-screening process. Promising candidates can then be identified for extensive follow-up using our combined experimental and modeling approaches. REST simulations of the (more computationally expensive) full PEPCANs could then be performed for the most promising peptide sequences, where our other two metrics, $N_{\text{CN-low}}$ and SASA_{NP}, and others that remain to be identified, may be evaluated in detail. This strategy is expected to be successful for other Au NP/peptide combinations, and should be extensible to other noble metals. However, a universal applicability of this screening approach to a range of different NP materials remains to be demonstrated in future studies.

While our analysis of the surface contact score provides a means to identify peptides with low PEPCAN activation energies, this in itself does not reveal the characteristics associated with catalytically active peptide sequences. To probe this, we analyzed the structural characteristics of the adsorbed peptides in detail. In Tables S2 and S3, we summarize the degree of peptide-surface contact averaged over all chains of each PEPCAN, and the chain-by-chain breakdown of the residue-surface contact for A3, GBP1, and AgBP1. Strongly binding residues (based on previously reported amino-acid binding strengths)[55] are highlighted for the dodecapeptides in Table S2, and their distribution suggests that sequences that either feature a strong-binding residue distant from the chain ends (GBP1 and Pd4), or that feature a large separation (in the sequence) between strong-binding residues (Midas2), correlate with low activation energies. All peptides in our set with three or more strong-binding residues showed a good distribution along the chain length, and in a broad sense (*vide infra*) cannot satisfy these criteria; these all featured higher activation energies. This indicates that sequences that do not have a strongly pinned terminal chain segment, or do not have a strongly pinned central loop segment, facilitate lower activation energies. Intuitively, contingent upon these segments possessing backbone flexibility, then either of these characteristics would confer conformational variability of the peptide within these segments, conceivably facilitating the dynamic exposure of reactive sites on the Au NP. Sequences with pinning sites that are distributed along the chain length, such as AgBP1 and AuBP2, would not be able to provide this exposure.

One example that may appear counter-intuitive is the A3 sequence, because this sequence features a large sequential interval between pinning sites, but has a high activation energy. However, this central segment contains a double proline residue, a motif which is known to confer substantive backbone rigidity;[57] we propose that this segment rigidity obstructs dynamic surface exposure in this instance. In Table S3, the residue−surface contact on a chain-by-chain basis suggests that pinning sites tend to limit variability in the degree of contact across chains. Our hypothesis of conformational variability was also investigated via calculations of the degree of structural similarity between individual adsorbed peptide chains for the A3, AgBP1, and GBP1 PEPCANs, summarized in Table S14. The A3 chains share a substantially greater similarity with each other, compared with AgBP1 and GBP1, again indicating a higher degree of conformational invariance.

Our work illustrates the need to elucidate all aspects of the biotic/abiotic interface, including inorganic surface structural order, overall peptide overlayer morphology, and peptide-inorganic interactions to truly elucidate, predict, and potentially manipulate properties of peptide-enabled nanomaterial systems. Such atomic-scale detail is achievable through this rigorous experimental and computational approach, wherein experimental structural data or computational methods alone could not reliably guide the development of sequence-dependent structure/function relationships. As the 4-nitrophenol reduction mechanism takes place at the surface of the Au NPs, our approach can therefore be broadened to investigate a variety of energy-relevant and industrially relevant catalytic reactions, as well as other biotic-abiotic interactions of interest to sensing and optical applications. Taken together, this combined experimental/computational methodology can initiate the knowledge-based development of sequence-dependent structure/function relationships, which could open new vistas into the rational design of materials using peptide-enabled approaches.

■ CONCLUSIONS

Sequence-dependent structure/function relationships of peptide-enabled Au NPs, generated using environmentally benign synthetic routes, were analyzed through a combined experimental and computational approach. Atomic PDF analysis and RMC simulations provided experimentally determined NP configurations. These offered a basis for REST-MD simulations to obtain a complete, atomic-scale model for the peptide overlayer adsorbed on the Au NP surface, and subsequent assessment of factors contributing to its catalytic properties. Multiple aspects of the biotic/abiotic interface were found to influence catalytic activity, including the degree of binding of the peptide to the Au surface. In this regard, the findings from the resource-intensive REST-MD simulations of peptide overlayers on NP surfaces correlated very well with the outcomes from relatively cheaper REST-MD simulations of single peptide chains adsorbed on planar surfaces, indicating a potential screening approach for assessing peptides, prior to conducting more comprehensive experimental and computational analyses. The methodology demonstrated herein can readily be translated to other inorganic NP-peptide systems, paving the way for the development of rational sequence design rules for materials property enhancement.

■ ASSOCIATED CONTENT

Supporting Information

The Supporting Information is available free of charge on the ACS Publications website at DOI: 10.1021/jacs.5b09529.

DOI: 10.1021/jacs.5b09529
J. Am. Chem. Soc. 2016, 138, 540−548

Additional details regarding HE-XRD, PDF analysis, RMC modeling, REST-MD simulations, and resulting analysis of PDF/REST-MD generated configurations, including Sections S1−S7, Figures S1−S16, and Tables S1−S16 (PDF)

AUTHOR INFORMATION

Corresponding Authors

*nicholas.bedford@nist.gov
*rajesh.naik@us.af.mil
*knecht@miami.edu
*tiffany.walsh@deakin.edu.au

Notes

The authors declare no competing financial interest.
[×]N.M.B. and Z.E.H. contributed equally.

Present Address:

[•]Department of Chemistry, Georgia Southern University, Statesboro, Georgia, 30460, United States.

ACKNOWLEDGMENTS

This work was partially supported by the Air Force Office for Scientific Research (M.R.K. and T.R.W., Grant No. FA9550-12-1-0226; R.R.N., AFOSR LRIR) and DOE-BES grant DE-SC0006877 (V.G.P.). N.M.B. acknowledges fellowship support from the National Research Council Research Associateship award during the initial experiments of this study. T.R.W. thanks **veski** for an Innovation Fellowship. T.R.W. and Z.E.H. gratefully acknowledge the National Computing Infrastructure (NCI) for access to supercomputing resources. Access to beamline 11-ID-C of the Advanced Photon Source, a U.S. Department of Energy (DOE) Office of Science User Facility operated for the DOE Office of Science by Argonne National Laboratory under Contract No. DE-AC02-06CH11357, is greatly appreciated.

REFERENCES

(1) Mirkin, C. A.; Letsinger, R. L.; Mucic, R. C.; Storhoff, J. J. *Nature* **1996**, *382*, 607.
(2) Bedford, N. M.; Ramezani-Dakhel, H.; Slocik, J. M.; Briggs, B. D.; Ren, Y.; Frenkel, A. I.; Petkov, V.; Heinz, H.; Naik, R. R.; Knecht, M. R. *ACS Nano* **2015**, *9*, 5082.
(3) Kuang, Z.; Kim, S. N.; Crookes-Goodson, W. J.; Farmer, B. L.; Naik, R. R. *ACS Nano* **2010**, *4*, 452.
(4) Slocik, J. M.; Naik, R. R. *Adv. Mater.* **2006**, *18*, 1988.
(5) Park, S. Y.; Lytton-Jean, A. K. R.; Lee, B.; Weigand, S.; Schatz, G. C.; Mirkin, C. A. *Nature* **2008**, *451*, 553.
(6) Rothemund, P. W. K. *Nature* **2006**, *440*, 297.
(7) Chen, C.-L.; Rosi, N. L. *J. Am. Chem. Soc.* **2010**, *132*, 6902.
(8) Prozorov, T.; Mallapragada, S. K.; Narasimhan, B.; Wang, L.; Palo, P.; Nilsen-Hamilton, M.; Williams, T. J.; Bazylinski, D. A.; Prozorov, R.; Canfield, P. C. *Adv. Funct. Mater.* **2007**, *17*, 951.
(9) Kramer, R. M.; Li, C.; Carter, D. C.; Stone, M. O.; Naik, R. R. *J. Am. Chem. Soc.* **2004**, *126*, 13282.
(10) Douglas, T.; Strable, E.; Willits, D.; Aitouchen, A.; Libera, M.; Young, M. *Adv. Mater.* **2002**, *14*, 415.
(11) Schoen, A. P.; Schoen, D. T.; Huggins, K. N. L.; Arunagirinathan, M. A.; Heilshorn, S. C. *J. Am. Chem. Soc.* **2011**, *133*, 18202.
(12) Forbes, L. M.; Goodwin, A. P.; Cha, J. N. *Chem. Mater.* **2010**, *22*, 6524.
(13) Li, Y.; Tang, Z.; Prasad, P. N.; Knecht, M. R.; Swihart, M. T. *Nanoscale* **2014**, *6*, 3165.
(14) Chiu, C.-Y.; Li, Y.; Ruan, L.; Ye, X.; Murray, C. B.; Huang, Y. *Nat. Chem.* **2011**, *3*, 393.
(15) Lee, Y.; Kim, J.; Yun, D. S.; Nam, Y. S.; Shao-Horn, Y.; Belcher, A. M. *Energy Environ. Sci.* **2012**, *5*, 8328.
(16) Ruan, L.; Ramezani-Dakhel, H.; Lee, C.; Li, Y.; Duan, X.; Heinz, H.; Huang, Y. *ACS Nano* **2014**, *8*, 6934.
(17) Coppage, R.; Slocik, J. M.; Sethi, M.; Pacardo, D. B.; Naik, R. R.; Knecht, M. R. *Angew. Chem., Int. Ed.* **2010**, *49*, 3767.
(18) Coppage, R.; Slocik, J. M.; Ramezani-Dakhel, H.; Bedford, N. M.; Heinz, H.; Naik, R. R.; Knecht, M. R. *J. Am. Chem. Soc.* **2013**, *135*, 11048.
(19) Tang, Z.; Palafox-Hernandez, J. P.; Law, W.-C.; Hughes, Z. E.; Swihart, M. T.; Prasad, P. N.; Knecht, M. R.; Walsh, T. R. *ACS Nano* **2013**, *7*, 9632.
(20) Seker, U. O. S.; Wilson, B.; Dincer, S.; Kim, I. W.; Oren, E. E.; Evans, J. S.; Tamerler, C.; Sarikaya, M. *Langmuir* **2007**, *23*, 7895.
(21) Feng, J.; Slocik, J. M.; Sarikaya, M.; Naik, R. R.; Farmer, B. L.; Heinz, H. *Small* **2012**, *8*, 1049.
(22) Heinz, H.; Farmer, B. L.; Pandey, R. B.; Slocik, J. M.; Patnaik, S. S.; Pachter, R.; Naik, R. R. *J. Am. Chem. Soc.* **2009**, *131*, 9704.
(23) Palafox-Hernandez, J. P.; Tang, Z.; Hughes, Z. E.; Li, Y.; Swihart, M. T.; Prasad, P. N.; Walsh, T. R.; Knecht, M. R. *Chem. Mater.* **2014**, *26*, 4960.
(24) Pandey, R. B.; Heinz, H.; Feng, J.; Farmer, B. L.; Slocik, J. M.; Drummy, L. F.; Naik, R. R. *Phys. Chem. Chem. Phys.* **2009**, *11*, 1989.
(25) Akdim, B.; Pachter, R.; Kim, S. S.; Naik, R. R.; Walsh, T. R.; Trohalaki, S.; Hong, G.; Kuang, Z.; Farmer, B. L. *ACS Appl. Mater. Interfaces* **2013**, *5*, 7470.
(26) Pacardo, D. B.; Sethi, M.; Jones, S. E.; Naik, R. R.; Knecht, M. R. *ACS Nano* **2009**, *3*, 1288.
(27) Naik, R. R.; Stringer, S. J.; Agarwal, G.; Jones, S. E.; Stone, M. O. *Nat. Mater.* **2002**, *1*, 169.
(28) Brown, S. *Nat. Biotechnol.* **1997**, *15*, 269.
(29) Kim, J.; Rheem, Y.; Yoo, B.; Chong, Y.; Bozhilov, K. N.; Kim, D.; Sadowsky, M. J.; Hur, H.-G.; Myung, N. V. *Acta Biomater.* **2010**, *6*, 2681.
(30) Peelle, B. R.; Krauland, E. M.; Wittrup, K. D.; Belcher, A. M. *Langmuir* **2005**, *21*, 6929.
(31) Hnilova, M.; Oren, E. E.; Seker, U. O. S.; Wilson, B. R.; Collino, S.; Evans, J. S.; Tamerler, C.; Sarikaya, M. *Langmuir* **2008**, *24*, 12440.
(32) Hnilova, M.; Liu, X.; Yuca, E.; Jia, C.; Wilson, B.; Karatas, A. Y.; Gresswell, C.; Ohuchi, F.; Kitamura, K.; Tamerler, C. *ACS Appl. Mater. Interfaces* **2012**, *4*, 1865.
(33) Terakawa, T.; Kameda, T.; Takada, S. *J. Comput. Chem.* **2011**, *32*, 1228.
(34) Wright, L. B.; Walsh, T. R. *Phys. Chem. Chem. Phys.* **2013**, *15*, 4715.
(35) Habchi, J.; Tompa, P.; Longhi, S.; Uversky, V. N. *Chem. Rev.* **2014**, *114*, 6561.
(36) Baker, C. M.; Best, R. B. *WIREs Comput Mol Sci* **2014**, *4*, 182.
(37) Hughes, Z. E.; Walsh, T. R. *J. Mater. Chem. B* **2015**, *3*, 3211.
(38) Wright, L. B.; Palafox-Hernandez, J. P.; Rodger, P. M.; Corni, S.; Walsh, T. R. *Chem Sci* **2015**, *6*, 5204.
(39) Brown, A. H.; Rodger, P. M.; Evans, J. S.; Walsh, T. R. *Biomacromolecules* **2014**, *15*, 4467.
(40) Wunder, S.; Polzer, F.; Lu, Y.; Mei, Y.; Ballauff, M. *J. Phys. Chem. C* **2010**, *114*, 8814.
(41) Chan, W. C.; White, P. D. *Fmoc Solid Phase Peptide Synthesis: A Practical Approach*; Oxford University Press: New York, 2000.
(42) Petkov, V. *J. Appl. Crystallogr.* **1989**, *22*, 387.
(43) Gereben, O.; Petkov, V. *J. Phys.: Condens. Matter* **2013**, *25*, 454211.
(44) Wyckoff, R. W. G. *Crystal Structures 1, 2nd Edition*, Interscience Publishers: New York, 1963, 85−237.
(45) Frenkel, A. I.; Yevick, A.; Cooper, C.; Vasic, R. *Annu. Rev. Anal. Chem.* **2011**, *4*, 23.
(46) Hess, B.; Kutzner, C.; van der Spoel, D.; Lindahl, E. *J. Chem. Theory Comput.* **2008**, *4*, 435.
(47) Petkov, V. *Mater. Today* **2008**, *11*, 28.
(48) Petkov, V.; Ren, Y.; Shan, S.; Luo, J.; Zhong, C.-J. *Nanoscale* **2014**, *6*, 532.

DOI: 10.1021/jacs.5b09529
J. Am. Chem. Soc. 2016, 138, 540−548

(49) Metropolis, N.; Rosenbluth, A. W.; Rosenbluth, M. N.; Teller, A. H.; Teller, E. *J. Chem. Phys.* **1953**, *21*, 1087.
(50) Keen, D. A.; Mcgreevy, R. L. *Nature* **1990**, *344*, 423.
(51) Le Roux, S.; Martin, S.; Christensen, R.; Ren, Y.; Petkov, V. *J. Phys.: Condens. Matter* **2011**, *23*, 035403.
(52) Skinner, L. B.; Huang, C.; Schlesinger, D.; Pettersson, L. G. M.; Nilsson, A.; Benmore, C. J. *J. Chem. Phys.* **2013**, *138*, 074506.
(53) Petkov, V.; Bedford, N.; Knecht, M. R.; Weir, M. G.; Crooks, R. M.; Tang, W.; Henkelman, G.; Frenkel, A. *J. Phys. Chem. C* **2008**, *112*, 8907.
(54) Petkov, V.; Lee, Y.; Sun, S.; Ren, Y. *J. Phys. Chem. C* **2012**, *116*, 26668.
(55) Feng, J.; Pandey, R. B.; Berry, R. J.; Farmer, B. L.; Naik, R. R.; Heinz, H. *Soft Matter* **2011**, *7*, 2113.
(56) Slocik, J. M.; Stone, M. O.; Naik, R. R. *Small* **2005**, *1*, 1048.
(57) Notman, R.; Oren, E. E.; Tamerler, C.; Sarikaya, M.; Samudrala, R.; Walsh, T. R. *Biomacromolecules* **2010**, *11*, 3266.

DOI: 10.1021/jacs.5b09529
J. Am. Chem. Soc. 2016, 138, 540−548